Structure of whispering gallery mode spectrum of microspheres coated with fluorescent silicon quantum dots

Y. Zhi,[1] J. Valenta,[2] and A. Meldrum[1,*]

[1]*Department of Physics, University of Alberta, Edmonton, Alberta T6G2E1, Canada*
[2]*Department of Chemical Physics and Optics, Charles University, Ke Karlovu 3, Prague, Czech Republic*
**Corresponding author: ameldrum@ualberta.ca*

Received July 26, 2013; accepted September 29, 2013;
posted October 10, 2013 (Doc. ID 194668); published October 31, 2013

Whispering gallery modes (WGMs) in microspheres containing embedded fluorophores (e.g., organic dyes or quantum dots) may find refractometric sensing or microlasing applications. However, there have been relatively few investigations on the relationship between the intrinsic microsphere resonances and the WGMs observed in fluorescence spectra for emitters coupled to the microsphere. Here we find that an apparently simple fluorescence WGM spectrum can mask a much more complicated underlying microcavity mode structure and that the observed fluorescence spectra are controlled by the emitter linewidth. By examining the cavity structure, we also verify that an effective ensemble emitter linewidth can be extracted from the fluorescence data. Finally, spectral diffusion is suggested as a possible origin of the periodic fluorescence WGM spectra observed in many microsphere cavities, without which these resonances might be unobservable.

OCIS codes: (160.4236) Nanomaterials; (230.5750) Resonators; (140.3948) Microcavity devices; (160.2540) Fluorescent and luminescent materials.
http://dx.doi.org/10.1364/JOSAB.30.003079

1. INTRODUCTION

Optical microcavities provide a means to control the luminescence of semiconductor quantum dots (QDs). In the strong cavity-coupling regime, QDs may be used as photon sources for quantum computation experiments [1–4]. However, strongly coupled systems in which single QDs interact with a microcavity are difficult to realize experimentally. In contrast, weak dissipative cavity coupling for ensembles of QDs is simple to achieve. In this regime, the spontaneous emission rates are modified by the optical density of states in the cavity. These systems are currently being explored for the development of microlasers [5–8], sensitive optical [9] and chemical microsensors [10–13], and microfluidics [14–16]. Weakly coupled systems may even find specific applications in quantum logic [17]. Thus the basic physics of ensemble QD–cavity interactions in the weak-coupling regime is of fundamental and technical importance. Nevertheless, there are relatively few examples in which the fluorescence spectrum is clearly related to the intrinsic cavity modes. This relationship can lead to a better understanding of the fluorescence whispering gallery mode (WGM) structure, as well illustrated in one recent example [18].

Here we explore the interactions of an ensemble of silicon QDs (Si QDs) coupled to the WGMs of a microsphere cavity. The WGMs are characterized by a radial mode number, n, which defines the number of intensity maxima in the radial direction, and angular numbers l and m ($m = -l, -l+1, \ldots, +l$), which define the number of maxima in the azimuthal and polar directions. The initial motivation was provided by observations that the WGM quality (Q) factors (Q-factor $= \lambda_{\text{peak}}/\Delta\lambda$, where λ_{peak} is central wavelength and $\Delta\lambda$ is spectral linewidth) observed in the fluorescence spectrum for modes with different l were apparently lower than the bare cavity Q-factors, an observation that we [19] and others [20] previously attributed to the effect of the QD homogeneous linewidth. However, these recent efforts left open some important questions. First, the dot linewidth required to produce the observed fluorescence spectra was much narrower (1–3 meV) than the linewidths observed experimentally from single Si QDs at room temperature (~150 meV). This problem is similar to that initially reported in studies of dye-doped droplets, over 20 years ago [21]. Second, the fluorescence free spectral range (FSR) was orders of magnitude larger than the 30 GHz scan width of the tunable lasers used in previous experiments [22]. Thus the cavity modes observed via evanescent coupling could not be directly related to the resonances in the fluorescence spectrum.

The purpose of the present work is to achieve a better understanding of the fluorescence WGM structure, especially as it relates to the mode structure of the "cold" cavity. The effects of the intrinsic QD linewidth, the transfer function of the spectroscopy system, and intra-QD processes, such as spectral diffusion, tunneling, and resonance energy transfer can all contribute to the observed fluorescence WGMs.

2. EXPERIMENTAL

Microspheres were fabricated by melting the end of a fiber taper using a CO_2 laser. They were then coated with a layer of Si QDs embedded in a silicon oxide matrix, using previously described methods [23]. In short, the microspheres were dipped vertically into a solution of hydrogen silsesquioxide (HSQ) in a methyl isobutyl ketone solution. They were then

dried in nitrogen and annealed at a temperature of 1100°C for 1 h in flowing $N_2 + 4\%H_2$ gas to produce oxide film with embedded Si QDs.

Fluorescence spectroscopy was performed by pumping the QDs with an Ar^+ ion laser operated at a wavelength of 488 nm. The fluorescence was collected by a microscope objective and imaged onto the entrance slit of a spectrometer with a pitch of 0.066 nm/pixel (the Lhires from Shelyak Instruments). Fluorescence experiments were performed also at cryogenic temperatures using another micro-spectroscopy setup. For these measurements, the pump source was a 405 nm diode laser, which was coupled to an optical cryostat (Janis ST-500) and an imaging spectrometer (Acton SP-2300i) with a LN-cooled CCD camera.

Bare cavity transmission measurements were performed using the standard method by tapering an optical fiber and bringing the microsphere within the evanescent field of the taper. Light from a Newport TLB-series tunable laser was injected into the taper, evanescently coupled to the microsphere, and the transmission intensity was measured using a photodiode. Part of the beam was picked off with a splitter and sent to a Burleigh 1000 wave meter. The laser can mechanically scan between 765 and 781 nm without mode hops, thus minimizing unpredictable wavelength jumps. A half-wave plate was used to control the polarization of the light in the fiber taper.

3. RESULTS AND ANALYSIS

A representative microsphere is shown in Fig. 1. Its diameter is about 50 μm, and it exhibits the red fluorescence, which is typical of Si QDs. The PL intensity is somewhat nonuniform along the polar directions, possibly due to thickness variations caused by the vertical dipping during sample preparation. However, the intensity around the equator is fairly constant, suggesting that the film is uniform in the regions used for data collection. The mode structure from fluorescence measurement in both TE and TM polarizations is also shown, where the TE/TM polarization corresponds to the electric field perpendicular/parallel to the WGM plane. The TE modes are characterized by Q-factor of up to ~1000, a visibility of ~0.6, an FSR of 2.87 nm, and a finesse of 7.4. The modes appear asymmetric (Fig. 1 inset), with a slight skewing toward longer wavelengths. The TE polarized fluorescence WGMs appear much stronger than the TM ones, but this was mainly a result of a strong difference in the polarization efficiency of the optics in the microscope and spectrometer. By direct imaging on a different system, the two polarizations were found to have a roughly similar intensity. For TM modes, the Q-factor, visibility, FSR, and finesse is ~840, 0.15, 3.06 nm, and 6.7, respectively. Normally, one might assume that these are first-radial-order ($n = 1$) resonances and identify them by solving the characteristic equations [24,25] for a coated sphere of the observed radius of ~25 μm. However, as we will show below, this may not represent an adequate mode identification.

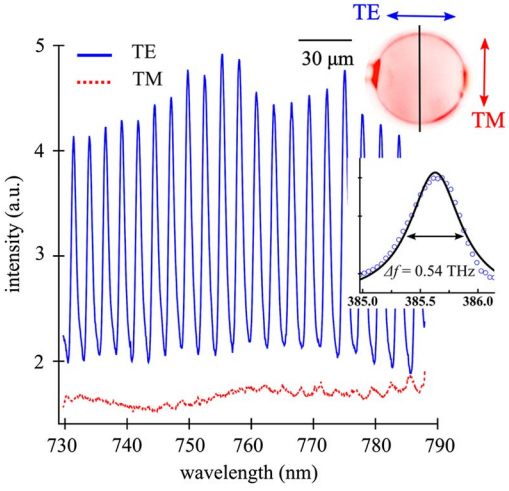

Fig. 1. TE- and TM-polarized fluorescence spectra of the QD-coated microsphere. The upper inset shows a fluorescence image of the microsphere, with the orientation of TE and TM polarization directions shown. The vertical line indicates the entrance slit position of the spectrometer. The lower inset shows one mode cropped from the spectrum and the corresponding best-fit Lorentzian curve. The inset scale is converted to THz units.

The transmission WGM structure (from evanescent measurements on the same microsphere) depended on the distance between the fiber taper and the sample (Fig. 2). When the sphere and the taper were well-separated (undercoupled), the Q-factor for this mode was $\sim 6.0 \times 10^5$, as measured by fitting a Lorentzian curve to the data. As the sphere and the taper were brought closer together, the transmission minima first deepened and then became wider as the system transitioned to the overcoupled regime. Finally, when the taper and the sphere were in physical contact, the Q-factor of the individual mode shown in Fig. 2 decreased to $\sim 2 \times 10^5$, while the overall background transmission level also decreased strongly. Attractive forces caused the taper to suddenly "snap" into contact with the sphere when they were

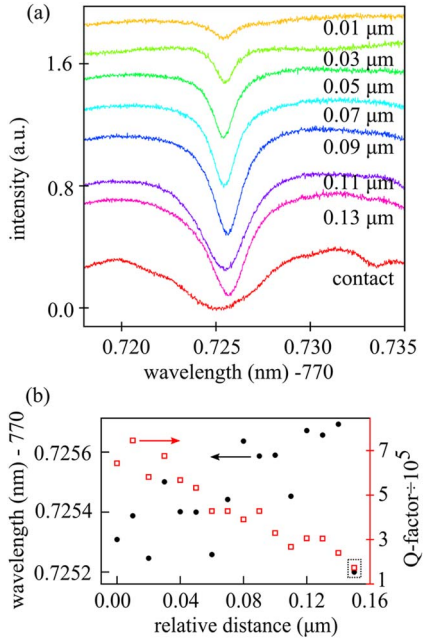

Fig. 2. (a) Subset of transmission spectra taken as the distance between the taper and the microsphere was reduced. (b) The central wavelength (circles) and Q-factor (squares) as a function of distance moved, as the taper approached the microsphere. The two points inside the dashed square indicates sphere-taper contact. Because the taper eventually snaps into contact with the microsphere, the horizontal axis indicates the distance moved relative to the location of the initial spectrum. Graphs (b) show the full data set; in (a) only a subset is shown for space reasons.

close together, which made it difficult to accurately determine the absolute distance between them. Therefore, Fig. 2 uses a relative distance scale.

Figures 1 and 2 are consistent with previous results that appeared to show a considerable difference between the fluorescence and transmission mode structure [16,26]. The mode shown in the transmission scan has a Q-factor that is orders of magnitude greater than that observed in the fluorescence spectrum. However, the 30 GHz piezo-scan limitation restricts the number of observable cavity modes, making it difficult to unambiguously identify them or establish their relationship with the WGMs shown in Fig. 1.

In order to establish the relationship between the cavity and fluorescence WGM spectra more clearly, a set of mechanical scans were taken in the range between 765 and 781 nm at a sampling rate of 0.2 pm per point. These spectra were acquired in the undercoupled regime, so as to minimize taper-induced losses from the cavity. A half-wave plate was used to control the polarization of the light entering the taper. Video images taken of light scattered from the taper and passed through an analyzer unambiguously determined the polarization (TE or TM) with respect to the plane of the microsphere's equator.

The transmission spectra indicated that the cavity mode structure is more complicated than would be expected on the basis of the fluorescence WGMs alone (Fig. 3). In both polarizations, the spectra consisted of closely spaced families of modes. Individual WGMs within these families were separated by approximately 45 pm [see Figs. 3(a2) and 3(b2)]. The Q-factors were estimated by performing Lorentzian fits and were found to be generally in the range of 10^5 for both sets of mode families. The maximum achievable Q-factor is probably limited by surface roughness, as well as scattering and absorption in the QD film, since we have measured values approaching 10^9 in uncoated microspheres fabricated with the same method [26].

The observed modes were identified by first modeling the spectrum using the perturbation theory methods developed by Teraoka and Arnold [24,25]. Accordingly, for the TE case

$$E_l(r) = \begin{cases} A_l\psi_l(n_1kr) & r < a-t \\ B_l\psi_l(n_2kr) + C_l\xi_l^1(n_2kr) & a-t < r < a \\ D_l\xi_l^1(n_3kr) & r > a \end{cases}. \quad (1)$$

In Eq. (1), n_1, n_2, and n_3 are the refractive indices of the microsphere ($n_1 = 1.452$), the QD film ($n_2 = 1.670$), and outside air ($n_3 = 1.000$), respectively, and ψ_l and ξ_l^1 are the lth spherical Riccati–Bessel and Riccati–Hankel functions, and A_l, B_l, C_l, and D_l are proportionality constants. $\psi_l(n_2kr)$ can be replaced by $\xi_l^2(n_2kr)$ to model the incoming wave in the middle layer, but it has a negligible effect on a structure of this size. The boundary conditions for TE polarization (the field amplitude and its derivatives must be continuous) lead to the solutions for the resonance wave vectors k. These are given by the roots of the expression [24]

$$\frac{n_3\xi_l^{1'}(n_3ka)}{n_2\xi_l^1(n_3ka)} = \frac{(B_l/C_l)\psi_l'(n_2ka) + \xi_l^{1'}(n_2ka)}{(B_l/C_l)\psi_l(n_2ka) + \xi_l^1(n_2ka)} \quad (2)$$

in which the primes indicate the derivative with respect to the argument, as usual. Here, the ratio of the pre-factors is given by

$$(B_l/C_l) = \frac{n_2\psi_l(n_1k(a-t))\xi_l^{1'}(n_2k(a-t)) - n_1\psi_l'(n_1k(a-t))\xi_l^1(n_2k(a-t))}{-n_2\psi_l(n_1k(a-t))\psi_l'(n_2k(a-t)) + n_1\psi_l'(n_1k(a-t))\psi_l(n_2k(a-t))}. \quad (3)$$

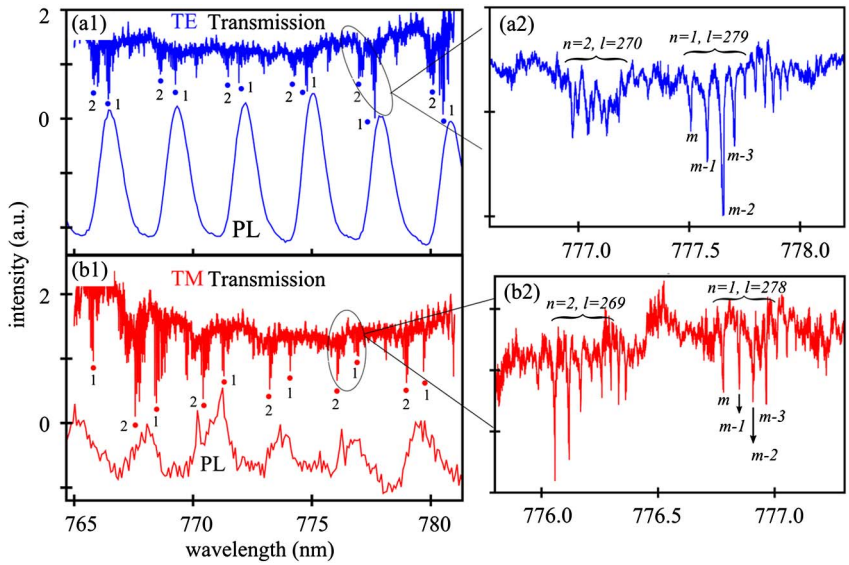

Fig. 3. Transmission and photoluminescence (PL) spectra for the QD-coated microsphere. Both (a) TE and (b) TM polarizations are shown. The fluorescence WGMs correspond to groups of transmission modes. The slight wavelength mismatch may be due to the different calibration procedures required to obtain the two types of spectra. The zoom-ins (a2) and (b2) show an expanded view of two of the transmission mode families.

The solutions for Eq. (2) were found using a numerical solver written in Mathematica [27]. Thus it is straightforward to find the mode Q-factors ($Q = \mathrm{Re}[k]/2\,\mathrm{Im}[k]$) associated with the radiation losses or with lossy materials. The TM case is mathematically very similar (with different boundary conditions) [25], so those equations will not be repeated here.

A good match to the data was found for a sphere radius of 24.7 μm and a film thickness of 50 nm. Considering only radiation losses, one would expect the highest Q-factors to be associated with the first radial order ($n = 1$) modes, but the presence of a lossy surface layer can alter this relationship. Figures 4(a) and 4(b) show the electric field profiles for the TE and TM polarized WGMs, respectively. In both cases, the main Q-limiting mechanism was found to be associated with the QD layer. For example, in the TE case [Fig. 4(a)] both $n = 1$ and $n = 2$ radial mode fields overlap to a roughly similar extent with the QD layer, so the Q-factors for both modes are similarly limited by absorption and scattering losses. They also both experience a similar surface-roughness-induced scattering. The theoretical results yielded Q-factors close to 10^5 for the $n = 1$ and $n = 2$ WGMs, which is consistent with the observations in Fig. 3. The modeling also gave a higher Q-factor for the TM polarization, owing to a smaller overlap with the QD layer [Fig. 4(b)], also in agreement with the results shown in Fig. 3 (the experimental TM Q-factors averaged about 1×10^5, compared to 6×10^4 for the TE case). The resonance shown in Fig. 2 is likely a higher-radial-order TM mode, which for these conditions can have Q-factors closer to 10^6.

Surface roughness also can affect the ultimate cavity Q-factors achievable in these coated structures. While $Q = 10^6$ is an approximate upper limit in Si-QD-coated microspheres, in the uncoated case we have measured values of about 4×10^8. While atomic force microscopy (AFM) is rather difficult due to the fragility of these structures, Bianucci *et al.* [22] found an RMS roughness of 3.4 nm, using AFM on a flat QD film made by the same technique. This leads to a (very approximate) roughness limited Q-factor of about 10^5 for a microsphere of this radius, according to the methods used in [28].

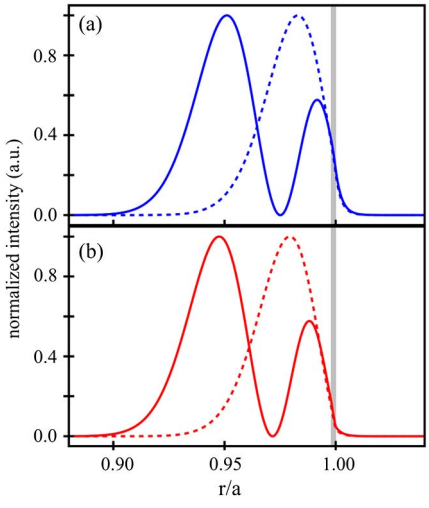

Fig. 4. (a) Intensity profile of the first- and second-order radial TE modes with angular orders $l = 279$ and $l = 270$, respectively, where r and a on the horizontal axis represent the radial distance from the center of the sphere and the sphere's radius, respectively. Resonant wavelengths are 777.58 and 777.04 nm. (b) Intensity profiles of the first- and second-order radial TM modes with $l = 278$ and $l = 269$, respectively. Resonant wavelengths are 777.46 and 777.05 nm. In both (a) and (b), the dashed line represents the first-order-radial mode, and the solid line represents the second-order-radial mode. The QD film is represented by the vertical shaded line.

The splitting of these resonances into families of closely spaced modes is attributed to a very slight prolate distortion of the microsphere, which breaks the degeneracy of modes having a different number of polar maxima (i.e., modes with different values of m) [29]. An image analysis of the microsphere taken in transmitted light suggested a very slight prolate eccentricity of about 0.01. This is in agreement with previous work on uncoated microspheres fabricated using the same method [30,31]. Given a mode degeneracy splitting of ~45 pm, the distortion amplitude can be estimated as [31] $e = l \cdot \Delta f / f = 0.016$, corresponding to an eccentricity of approximately 0.008, in reasonable agreement with observation.

The cavity mode structure was then compared to the fluorescence spectra (see Fig. 3). While the scaling is imperfect due to the different wavelength calibrations used in each type of measurement, the fluorescence WGMs are mainly coincident with the groups of mode families observed in the transmission results for both polarizations. The fluorescence spectra therefore consist of a nearly equal mixture of both radial orders. Thus, the apparently single WGMs in the fluorescence spectrum correspond to multiplets of overlapping cavity modes with much higher Q-factors. The asymmetry of the fluorescence WGMs, which hinders the Lorentzian line fitting (e.g., see Fig. 1) could arise from the structure of the underlying families of cavity modes. The similarity of the Q-factors for the first and second order modes is in contrast to previous experiments [16] in which the first-order modes dominated the fluorescence spectrum. However, the previous work used water as the external medium, in which case Eqs. (1)–(3) do predict that the first-order modes would have a much higher Q-factor.

The results confirm that the fluorescence Q-factors are lower than the cold cavity values in the same microsphere. In fact, much of the WGM substructure is totally washed out in the fluorescence spectra, leaving what appears to be only a single broad WGM at each apparent resonance. This effect could arise from two sources: (1) the transfer function of the spectrometer system may wash out the high-resolution mode structure (i.e., the fine structure really exists in the emitted fluorescence but cannot be resolved) or (2) the finite QD linewidth may lead to a spectrally broadened Purcell enhancement causing extensive mode overlap (i.e., the bare cavity mode structure is intrinsically washed out, due to the QD linewidth).

The first possibility was investigated by measuring the spectrometer transfer function using a spectral line from an Hg–Ar calibration lamp. The transmission spectrum in Fig. 3(a2) was then convolved with the transfer function to produce the resulting simulated fluorescence spectrum (Fig. 5). While the fine mode structure is indeed washed out, the result does not resemble the real fluorescence WGM data. The first- and second-order mode families appear as a broad but clear doublet, which is not observed in the fluorescence spectrum. In contrast, convolving a 1.6 meV QD linewidth (i.e., the calculated linewidth based on [19], as discussed further below) causes the entire set of cavity modes

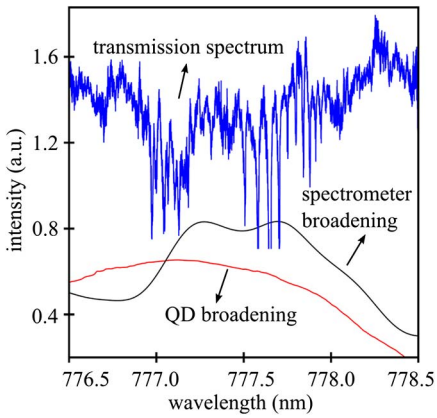

Fig. 5. TE transmission spectrum (blue line), shown along with its convolution with the spectrometer transfer function (black line) or with a QD linewidth of 1.6 meV (red line). The results were inverted to simulate a fluorescence spectrum. The spectrometer transfer function results in a broad, double-peaked mode, while a QD linewidth convolved with the transmission spectrum would result in a single, slightly asymmetric fluorescence maximum, similar to the experimental observation.

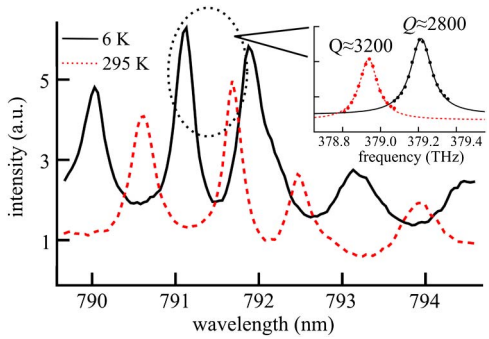

Fig. 6. PL spectra of a QD-coated microsphere at 6 K (solid line) and 295 K (dashed line), respectively. The inset shows the Lorentzian fitting of one mode.

around 777 nm to appear as a single peak, similar to the actual fluorescence spectrum. Thus one can conclude that the fluorescence WGM linewidth is not limited by the spectrometer transfer function, but is indeed due to the QD–cavity coupling.

The QD linewidth required to produce fluorescence WGMs with $Q = 1000$–3000 can be estimated [19] as $\Delta\lambda_{QD} \approx \lambda_{peak}/Q + \Delta\lambda_{cav} \approx 260$–$780$ pm or approximately 0.5–2 meV ($\Delta\lambda$ indicates the spectral linewidth of the QD or the cavity, as indicated by the subscript). However, this estimated linewidth is much narrower than the reported room-temperature linewidth of single Si QDs, which is in the range of 150 meV [32–34]. Indeed, for such a large QD linewidth, which is comparable to or greater than the FSR, no modes should be visible in the fluorescence spectra at all.

One possible explanation for this apparent inconsistency is related to spectral diffusion (SD) in the QDs. SD causes the relatively narrow homogeneous linewidth of a single particle to randomly jump or diffuse about a distribution of emission energies, making the time-averaged linewidth appear broad. Spectral diffusion has been well studied in direct-gap QDs [35] and is attributed to a crystal-field distortion arising from charge trapping within excited particles [36]. At low temperature, the time scale for the SD process can be on the order of milliseconds or even seconds in capped QDs [37], although it can be faster depending on the surface conditions [38]. The SD rate increases at elevated temperature, owing partly to thermally activated escape from local trap sites [35]. Thus many studies focus on spectral diffusion at low temperature in order to avoid thermal effects, which tend to dominate at temperatures above 50 K, at least in CdSe QDs [39]. There is one previous report of SD in Si QDs, in which the single-particle linewidth narrowed from 150 to 105 meV when the collection time was shortened by a factor of 100, at room temperature [34]. More recent reports have shown that individual luminescence spectra of Si-QDs can jump over a range of about 100 meV [40,41]. Thus spectral diffusion could play an important role in the observed fluorescence WGM spectra.

In order to investigate an SD-related explanation for the WGM spectra reported here, a QD-coated microsphere was cooled to 6 K (this was a different microsphere than the one shown above). At low temperatures, the line-broadening effects of SD should be minimized. Figure 6 illustrates how the fluorescence spectra changed as a function of temperature in these experiments. First, the WGMs red-shifted as the temperature increased from 6 to 295 K. This effect has been observed before in glass microcavities and is attributed mainly to the positive thermo-optic and thermal expansion coefficients of silica [42,43]. More interestingly from the point of view of the spectral diffusion hypothesis, the fluorescence Q-factor *increased* from ~2800 to ~3200) on heating from 6 K up to room temperature while the mode visibility (essentially derived from the peak-to-background ratio) also slightly increased.

A higher Q-factor at elevated temperatures seems surprising, but it can be explained on the basis of spectral diffusion. At low temperatures, SD is minimized and, in an extreme limiting case, the QD homogeneous emission would be frozen in. Under these conditions, the model [19] developed previously would apply, and a homogeneous QD linewidth of about 0.5 meV would be needed to produce the observed low-temperature spectrum, which agrees reasonably well with single-particle spectroscopy results at low temperature [33]. As the temperature is increased, SD processes would become faster and extend over a broader energy range [44]. As previously suggested for dye droplets [45], random spectral diffusion could increase the on-resonance emission probability, since a normally "off resonance" emitter can undergo spectral diffusion toward a resonance, where the emission rate is faster. This changes the smooth probability distribution for emitted photons from the whole QD ensemble, instead giving a rippled distribution in which emission is more likely to occur on a cavity resonance than it would be in the absence of SD.

The possible effect of SD on the cavity luminescence can be illustrated with a simple back-of-the-envelope approximation. In [19], the ensemble PL spectrum was calculated as a smooth probability function representing an inhomogeneously broadened distribution of emitting particles, which was then perturbed by the cavity resonances. SD would alter the probability function by concentrating it more on resonance. In other words, a given QD is more likely to emit on resonance in the presence of SD than it would otherwise.

By using the model developed in [19] but altering the emission probability toward a cavity resonance, one finds a decrease in the intensity emitted far from the resonance and an apparent sharpening of the mode structure (Fig. 7). In the extreme limit, all of the particles would spectrally diffuse to the cavity resonance before they emit, resulting in an effectively

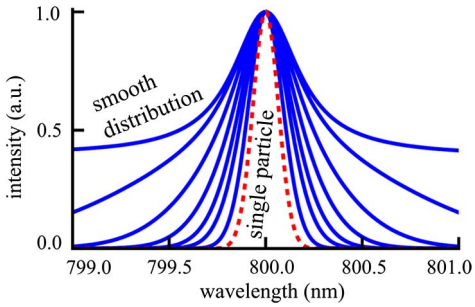

Fig. 7. Simulated fluorescence spectrum from a single cavity mode with $Q = 5 \times 10^5$ centered at 800 nm, for a QD linewidth of 0.8 meV. The peak becomes narrower as a greater fraction of the QDs emit closer to the cavity resonance. The spectrum would eventually become equivalent to that for a single particle centered on resonance (dashed red line). The Q-factor in that case is close to the estimated value for a single particle, given by $Q = \lambda_{\text{peak}}/(\Delta\lambda_{\text{QD}} - \Delta\lambda_{\text{cavity}})$.

single-particle emission spectrum. While one cannot determine how the emission probability distribution really looks from the experimental data, the effect of concentrating the distribution toward the cavity resonances clearly increases the apparent fluorescence Q-factor and the mode visibility.

The implications of SD can likely be extended to numerous QD–cavity systems operating at room temperature. For many different kinds of particles, ranging from Si [34] to InGaAs [46], to CdSe [35], the time-averaged single-particle linewidths at room temperature are much too wide to permit the existence of cavity modes in the ensemble fluorescence spectrum, despite the fact that the cavity resonances are almost always observable. Although the effects of SD in fluorescent microcavities were originally suggested many years ago [45] and are probably ubiquitous in these cavity-coupled systems, SD has not been much considered in terms of the basic physics of ensemble QD–cavity interactions in the weak coupling regime. In fact, it seems that without SD, many QD–cavity systems might not show fluorescence WGMs at room temperature at all.

These results have some implications for the development of light emitters and sensors based on Si-QD-coated microcavities. We did not find clear evidence for stimulated emission or lasing under any of the conditions investigated (e.g., no line narrowing or sudden increases in output intensity of certain modes as a function of pump power) up to about 200 mW laser power focused in free-space to the best of our ability onto the microsphere. Since we do not know the exact laser spot size at the microsphere location, it is difficult to estimate the power density exactly. A previous study using pulsed excitation did report evidence in favor of room-temperature ASE (amplified spontaneous emission) from a microsphere in which Si-QDs were deposited via a PECVD process [47]. While we cannot rule out the possibility of short time-scale stimulated emission from these observations, as also reported in flat films [48], we find that it probably does not occur in these samples under the strongest CW excitation we could reasonably achieve, with cavity Q-factors in the range of 10^5. These results also have potential implications in terms of the fluorescence WGM response in sensor-type devices as well, since the ultimate refractometric sensitivity may arise from the combined resonance shift of many underlying cavity modes.

4. CONCLUSIONS

This work investigated the whispering gallery mode spectrum of a quantum-dot coated microsphere. The bare cavity spectrum was found to have a much more complex structure than the relatively simple fluorescence spectrum. While we have previously attributed similar fluorescence WGM spectra to the first-order radial modes of the cavity, we find that the actual cavity structure consists of families of much higher Q resonances. Individual WGMs are split into overlapping groups of resonances due to the slight distortion of the microsphere. The assortment of modes is convolved into the broad resonances observed in the fluorescence spectrum, mainly as a result of the QD linewidth. At room temperature, the linewidth has to be less than 2 meV to produce the observed fluorescence WGM spectrum, for these Si QDs.

We also investigated the WGM structure at low temperatures. At 6 K, the fluorescence WGM Q-factors are slightly lower than they are at room temperature. This result is consistent with the possibility of spectral diffusion in the silicon QDs, or any other thermal process, which increases the on-resonance emission probability. SD would also explain why it is possible to observe modes at all, when the apparent single-dot linewidths are evidently so wide that they would otherwise have to completely wash out the WGM resonance structure.

These observations are probably applicable to many fluorescent microsphere structures in which the apparently simple fluorescence WGM structure masks a more complicated underlying cavity mode structure. Additionally, spectral diffusion (or a similar process) probably plays an important role in many emitter-cavity systems, since it can reconcile the apparently wide linewidths with the existence of WGMs in the emission spectra.

ACKNOWLEDGMENTS

The authors thank NSERC and AITF iCiNano for funding, and the Veinot Lab at the University of Alberta for providing some of the materials used in the coated microsphere synthesis. The work of one author (J. V.) was partially supported by the EU-project NASCEnT (FP7-245977). Y. Z. acknowledges partial support from the China Scholarship Council.

REFERENCES

1. C. Santori, D. Fattal, J. Vuckovic, G. S. Solomon, and Y. Yamamoto, "Indistinguishable photons from a single-photon device," Nature **419**, 594–597 (2002).
2. A. Kiraz, M. Atature, and A. Imamoglu, "Quantum-dot single-photon sources: prospects for applications in linear optics quantum-information processing," Phys. Rev. A **69**, 032305 (2004).
3. A. Dousse, J. Suffczynski, A. Beveratos, O. Krebs, A. Lemaitre, I. Sagnes, J. Bloch, P. Voisin, and P. Senellart, "Ultrabright source of entangled photon pairs," Nature **466**, 217–220 (2010).
4. T. D. Ladd and Y. Yamamoto, "Simple quantum logic gate with quantum dot cavity QED systems," Phys. Rev. B **84**, 235307 (2011).
5. S. I. Shopova, G. Farca, A. T. Rosenberger, W. M. S. Wickramanayake, and N. A. Kotov, "Microsphere whispering-gallery-mode laser using HgTe quantum dots," Appl. Phys. Lett. **85**, 6101–6103 (2004).
6. E. del Valle, S. Zippilli, F. P. Laussy, A. Gonzalez-Tudela, G. Morigi, and C. Tejedor, "Two-photon lasing by a single quantum dot in a high-Q microcavity," Phys. Rev. B **81**, 035302 (2010).
7. F. Albert, T. Braun, T. Heindel, C. Schneider, S. Reitzenstein, S. Hofling, L. Worschech, and A. Forchel, "Whispering gallery

mode lasing in electrically driven quantum dot micropillars," Appl. Phys. Lett. **97**, 101108 (2010).
8. G. C. Xing, Y. L. Liao, X. Y. Wu, S. Chakrabortty, X. F. Liu, E. K. L. Yeow, Y. Chan, and Y. T. C. Stun, "Ultralow-threshold two-photon pumped amplified spontaneous emission and lasing from seeded CdSe/CdS nanorod heterostructures," ACS Nano **6**, 10835–10844 (2012).
9. K. T. Posani, V. Tripathi, S. Annamalai, N. R. Weisse-Bernstein, S. Krishna, R. Perahia, O. Crisafulli, and O. J. Painter, "Nanoscale quantum dot infrared sensors with photonic crystal cavity," Appl. Phys. Lett. **88**, 151104 (2006).
10. A. Francois and M. Himmelhaus, "Whispering gallery mode biosensor operated in the stimulated emission regime," Appl. Phys. Lett. **94**, 031101 (2009).
11. H. T. Beier, G. L. Coté, and K. E. Meissner, "Modeling whispering gallery modes in quantum dot embedded polystyrene microspheres," J. Opt. Soc. Am. B **27**, 536–543 (2010).
12. S. Pang, R. E. Beckham, and K. E. Meissner, "Quantum dot-embedded microspheres for remote refractive index sensing," Appl. Phys. Lett. **92**, 221108 (2008).
13. H. A. Huckabay and R. C. Dunn, "Whispering gallery mode imaging for the multiplexed detection of biomarkers," Sens. Actuators B **160**, 1262–1267 (2011).
14. H. Zhu, J. D. Suter, I. M. White, and X. Fan, "Aptamer based microsphere biosensor for thrombin detection," Sensors **6**, 785–795 (2006).
15. C. P. K. Manchee, V. Zamora, J. Silverstone, J. G. C. Veinot, and A. Meldrum, "Refractometric sensing with fluorescent-core microcavities," Opt. Express **19**, 21540–21551 (2011).
16. Y. Zhi, T. Thiessen, and A. Meldrum, "Silicon quantum-dot-coated microspheres for microfluidic refractive index sensing," J. Opt. Soc. Am. B **30**, 51–56 (2013).
17. T. Yu, Y. Q. Ji, A. D. Zhu, H. F. Wang, and S. Zhang, "Robust teleportation and multipartite entanglement analyzers via quantum-dot spins in weak-coupling cavity quantum electrodynamics regime," J. Opt. Soc. Am. B **29**, 2029–2034 (2012).
18. B. Gayral and J. M. Gérard, "Photoluminescence experiment on quantum dots embedded in a large Purcell-factor microcavity," Phys. Rev. B **78**, 235306 (2008).
19. A. Meldrum, P. Bianucci, and F. Marsiglio, "Modification of ensemble emission rates and luminescence spectra for inhomogeneously broadened distributions of quantum dots coupled to optical microcavities," Opt. Express **18**, 10230–10246 (2010).
20. A. Pitanti, M. Ghulinyan, D. Navarro-Urrios, G. Pucker, and L. Pavesi, "Probing the spontaneous emission dynamics in Si-nanocrystals-based microdisk resonators," Phys. Rev. Lett. **104**, 103901 (2010).
21. M. D. Barnes, W. B. Whitten, S. Arnold, and J. M. Ramsey, "Homogeneous linewidths of rhodamine 6G at room temperature from cavity-enhanced spontaneous emission rates," J. Chem. Phys. **97**, 7842–7845 (1992).
22. P. Bianucci, X. Wang, J. Veinot, and A. Meldrum, "Silicon nanocrystals on bottle resonators: mode structure, loss mechanisms and emission dynamics," Opt. Express **18**, 8466–8481 (2010).
23. Y. Zhi, C. P. K. Manchee, J. Silverstone, Z. Zhang, and A. Meldrum, "Refractometric sensing with silicon quantum dots coupled to a microsphere," Plasmonics **8**, 71–78 (2013).
24. I. Teraoka and S. Arnold, "Enhancing sensitivity of a whispering gallery mode microsphere sensor by a high-refractive index surface layer," J. Opt. Soc. Am. B **23**, 1434–1441 (2006).
25. I. Teraoka and S. Arnold, "Whispering-gallery modes in a microsphere coated with a high-refractive index layer: polarization-dependent sensitivity enhancement of the resonance-shift sensor and TE-TM resonance matching," J. Opt. Soc. Am. B **24**, 653–659 (2007).
26. P. Bianucci, Y. Zhi, F. Marsiglio, J. Silverstone, and A. Meldrum, "Microcavity effects in ensembles of silicon quantum dots coupled to high-Q resonators," Phys. Status Solidi A **208**, 639–645 (2011).
27. http://www.wolfram.com.
28. R. D. Kekatpure and M. L. Brongersma, "Fundamental photophysics and optical loss processes in Si-nanocrystal-doped microdisk resonators," Phys. Rev. A **78**, 023829 (2008).
29. G. Chen, M. M. Mazumder, Y. R. Chemla, A. Serpengfizel, and R. K. Chang, "Wavelength variation of laser emission along the entire rim of slightly deformed microdroplets," Opt. Lett. **18**, 1993–1995 (1993).
30. G. Lin, B. Qian, Y. Candela, J.-B. Jager, Z. Cai, V. Lefévre-Seguin, and J. Hare, "Excitation mapping of whispering gallery modes in silica microcavities," Opt. Lett. **35**, 583–585 (2010).
31. V. Lefèvre-Seguin, "Whispering-gallery mode lasers with doped silica microspheres," Opt. Mater. **11**, 153–165 (1999).
32. J. Valenta, R. Juhasz, and J. Linnros, "Photoluminescence spectroscopy of single silicon quantum dots," Appl. Phys. Lett. **80**, 1070 (2002).
33. I. Sychugov, R. Juhasz, J. Valenta, and J. Linnros, "Narrow luminescence linewidth of a silicon quantum dot," Phys. Rev. Lett. **94**, 087405 (2005).
34. J. Martin, F. Chichos, and C. von Borczyskowski, "Spectral diffusion of quasi-localized excitons in single silicon nanocrystals," J. Lumin. **132**, 2161–2165 (2012).
35. S. A. Empedocles and M. G. Bawendi, "Influence of spectral diffusion on the line shapes of single CdSe nanocrystallite quantum dots," J. Phys. Chem. B **103**, 1826–1830 (1999).
36. A. Majumdar, E. D. Kim, and J. Vuckovic, "Effect of photogenerated carriers on the spectral diffusion of a quantum dot coupled to a photonic crystal cavity," Phys. Rev. B **84**, 195304 (2011).
37. P. Borri, W. Langbein, S. Schneider, U. Woggon, R. L. Sellin, D. Ouyang, and D. Bimberg, "Ultralong dephasing time in InGaAs quantum dots," Phys. Rev. Lett. **87**, 157401 (2001).
38. G. Sallen, A. Tribu, T. Aichele, R. André, L. Besombes, C. Bougerol, M. Richard, S. Tatarenko, K. Kheng, and J.-Ph. Poizat, "Subnanosecond spectral diffusion measurement using photon correlation," Nat. Photonics **4**, 696–699 (2010).
39. M. J. Fernée, T. Plakhotnik, Y. Louyer, B. N. Littleton, C. Potzner, P. Tamarat, P. Mulvaney, and B. Lounis, "Spontaneous spectral diffusion in CdSe quantum dots," J. Phys. Chem. Lett. **3**, 1716–1720 (2012).
40. I. Schyugov, J. Valenta, K. Mitsuishi, and J. Linnros, "Exciton localization in doped silicon nanocrystals from single dot spectroscopy studies," Phys. Rev. B **86**, 075311 (2012).
41. J. Valenta, A. Fucikova, F. Vacha, F. Adamec, J. Humpolickova, M. Hof, I. Pelant, K. Kusova, K. Dohnalova, and J. Linnros, "Light-emission performance of silicon nanocrystals deduced from single quantum dot spectroscopy," Adv. Funct. Mater. **18**, 2666–2672 (2008).
42. J. D. Suter, I. M. White, H. Zhu, and X. Fan, "Thermal characterization of liquid core optical ring resonator sensors," Appl. Opt. **46**, 389–396 (2007).
43. A. Tewary, M. J. F. Digonnet, J.-Y. Sung, J. H. Shin, and M. L. Brongersma, "Silicon-nanocrystal-coated silica microsphere thermo-optical switch," IEEE J. Sel. Top. Quantum Electron. **12**, 1476–1479 (2006).
44. J. Müller, J. M. Lupton, A. L. Rogach, J. Feldmann, D. V. Talapin, and H. Weller, "Monitoring surface charge migration in the spectral dynamics of single CdSe/CdS nanodot/nanorod heterostructures," Phys. Rev. B **72**, 205339 (2005).
45. H. Yukawa, S. Arnold, and M. Miyano, "Microcavity effect of dyes adsorbed on a levitated droplet," Phys. Rev. A **60**, 2491–2496 (1999).
46. K. Matsuda, T. Saiki, H. Saito, and K. Nishi, "Room-temperature photoluminescence spectroscopy of self-assembled $In_{0.5}Ga_{0.5}As$ single quantum dots by using highly sensitive near-field scanning optical microscope," Appl. Phys. Lett. **76**, 73–75 (2000).
47. H. Chen, J.-Y. Sung, A. Tewary, M. Brongersma, J. H. Shin, and P. M. Fauchet, "Evidence for stimulated emission in silicon nanocrystal microspheres," in *2nd IEEE International Conference on Group IV Photonics* (2005), pp. 99–101.
48. J. Ruan, P. M. Fauchet, L. Dal Negro, M. Cazzanelli, and L. Pavesi, "Stimulated emission in nanocrystalline silicon superlattices," Appl. Phys. Lett. **83**, 5479–5481 (2003).